Morphological Control of Anodic Crystalline TiO_2 Nanochannel Films for Use in Size-selective Photocatalytic Decomposition of Organic Molecules

E. Tsuji,[a,b,*] *Y. Taguchi,*[a] *Y. Aoki,*[a,b] *T. Hashimoto,*[c] *P. Skeldon,*[c] *G. E. Thompson*[c] *and H. Habazaki*[a,b]

a) Graduate School of Chemical Sciences and Engineering, Hokkaido University, Sapporo, Hokkaido 060-8628, Japan

b) Division of Materials Chemistry, Faculty of Engineering, Hokkaido University, Sapporo, Hokkaido, 060-8628, Japan

c) Corrosion and Protection Centre, School of Materials, The University of Manchester, Manchester, M13 9PL, England, United Kingdom

Corresponding author: Phone & Fax: +81-11-706-6736, e-mail: e-tsuji@eng.hokudai.ac.jp

Abstract

We report the size-selective photocatalytic decomposition of organic molecules using crystalline anodic TiO_2 nanochannel films as the photocatalyst. The porous TiO_2 films were formed by anodizing titanium at 20 V in glycerol electrolyte containing various amounts of K_3PO_4, K_2HPO_4, and KH_2PO_4 at 433 K. Regardless of the electrolyte composition, the as-formed TiO_2 films had a crystalline anatase structure. The basicity of the electrolyte markedly influenced the morphology of the TiO_2 nanochannel films; more regular nanochannels developed with increasing basicity of the electrolyte. Because the diameter of the nanochannels in the films formed in a basic electrolyte was as small as ~10 nm, the anodic TiO_2 nanochannel films with a thickness of 5 μm revealed a selective photocatalytic decomposition of methylene blue (MB) in a mixture of MB and direct red 80 (DR) kept under UV irradiation. The importance of the diameter of the nanochannels and their uniformity for size-selective decomposition of organic molecules were investigated.

Keywords

Anodizing, TiO_2 nanochannel films, size-selective photocatalysis, photocatalyst

1. Introduction

Selective photocatalytic reactions on semiconductor TiO_2 are challenging because TiO_2 is generally regarded as a nonselective photocatalyst for organic decomposition in aqueous solutions in the presence of air. The selectivity is critical when dealing with a mixture containing desirable as well as undesirable (toxic pollutants) compounds. Photocatalytic reactions on TiO_2 in water proceed by the following steps [1-4]: (i) generation of excited electron (e^-)-positive hole (h^+) pairs by absorption of UV light; (ii) production of hydroxyl radicals (•OH) by reaction of h^+ with surface -OH groups or adsorbed H_2O molecules; and (iii) oxidation of substrates by •OH on the TiO_2 surface. Because the oxidation of organic molecules by •OH is nonselective, the photocatalytic decomposition of organic molecules on TiO_2 is also generally nonselective.

Some researchers have improved the photocatalytic selectivity of TiO_2 mainly by two strategies: (i) controlling the adsorption properties by changing the crystal faces [4,5] and surface chemical groups [6], and (ii) hindering the passage of reactive molecules to TiO_2 using porous materials such as mesoporous silica [7,8] and mesoporous titanosilicate [3]. For example, to control the adsorption properties, Bai et al. investigated the selectivity of uniform anatase TiO_2 microspheres with a high percentage of exposed {001} facets for photocatalytic decomposition of methylene blue (MB) and methyl orange (MO) [4]. The •OH radicals thus generated on the TiO_2 surface were quite reactive. Therefore, the organic molecules that were easy to adsorb on the surface were preferentially oxidized by the •OH radicals. In this case, the degradation rate of MB was much faster than that of MO because of the preferred adsorption of MB on the {001}

facets. On the other hand, while investigating the suppression of the passage of reactive molecules, Inumaru et al. showed that nanocomposites of P25 TiO_2 nanoparticles and mesoporous silica showed molecular selective photocatalysis by controlling the pore size [8]. The nanocomposite catalysts with small pores (1.4–1.9 nm) decomposed heptylphenol (HP) faster than nonylphenols (NP), due to its diffusion rate into the small pores, whereas catalysts with large pores (2.7–5.3 nm) decomposed NP and HP at similar diffusion rates. Here, we demonstrate the size-selective decomposition of organic molecules using not nanocomposite films but only TiO_2 nanochannel films formed by anodizing titanium. In a mixture containing both small and large organic molecules, only the small molecules that could penetrate the nanochannels decomposed under UV irradiation.

Recently, we reported the formation of TiO_2 nanochannel films by anodizing titanium in hot phosphate/glycerol electrolytes [9-11]. The resultant films showed interesting features, for example: (i) the pore size was as small as ~10 nm leading to a high surface area, a preferable condition for fabricating an efficient photocatalyst; and (ii) formation of films at an anodizing voltage of 20 V generated the crystalline anatase phase without the requirement of post- annealing. Therefore, such anodic TiO_2 nanochannel films are of potential interest for fabricating flexible dye-sensitized solar cells (DSSCs) and electrochromic devices on plastic substrates.

However, the anodic TiO_2 nanochannel films reported previously had relatively disordered pore channels. Therefore, we report herein that the pore morphology of the anodic TiO_2 films formed in the hot phosphate/glycerol electrolytes was largely dependent on the basicity of electrolytes, and the TiO_2 films

with more regular cylindrical nanochannels were formed in the highly basic electrolytes. Size-selective photocatalytic decomposition was achieved by utilizing the crystalline TiO_2 regular cylindrical nanochannel films. To our knowledge, this is the first example of size-selective photocatalysis for small organic molecules using anodic TiO_2 nanochannels.

2. Experimental

The specimens used for anodizing comprised 99.5% pure titanium sheets of 0.5 mm thickness. Prior to anodizing, the specimens were electropolished in 1 mol dm^{-3} NaCl/ethylene glycol solution at 293 K at 20 V for 200 s and, subsequently, at 10 V for 600 s [12]. A titanium sheet was used as the counter electrode. The electropolished specimens were subsequently anodized in glycerol electrolyte containing phosphates such as K_3PO_4, K_2HPO_4, and KH_2PO_4 at 433 K under a nitrogen atmosphere. The total concentration of the phosphates was 0.8 mol dm^{-3}; the mixing ratios of the three phosphates are shown in Table 1. The electrolytes P1 and P5 show the highest and lowest basicity respectively. The conductivity of all electrolytes was almost the same with each other. The water content in the electrolyte was reduced to ~0.03 mass% by heating at 453 K under a dry nitrogen stream for 3 h. A platinum sheet was used as the counter electrode. For evaluating the crystallinity, the effective surface area, and photocatalytic activity for decomposition of organic molecules, ~5 μm thick films formed on the titanium sheets were used. For comparison of photocatalytic activity for decomposition of organic molecules, an anatase TiO_2 nanotubular film was also prepared as follows: the electropolished titanium specimen was anodized in 0.25 wt% NH_4F

and 1 vol% water/ethylene glycol electrolyte at 60 V for 45 min. Then, the resulting film was annealed at 723 K for 3 h in air for transformation from an amorphous to the anatase phase. Hereafter, this TiO_2 film is denoted as NT. The NT film of ~5 μm thickness had a nanotubular structure with pore diameters as large as ~100 nm, and the NT film was formed as a randomly oriented anatase crystal. The effective surface area of the NT film was about one fourth of that of the nanochannel films anodized in the P3 electrolyte, as reported previously [10]. In all the experiments, reagent-grade chemicals were used as-received; further the deionized water used was obtained from a Milli-Q water purification system.

The crystallinity of the anodic films was identified by X-ray diffraction (XRD; Rigaku, RINT-2000) with θ–2θ mode using Cu Kα radiation (40 kV, 20 mA). The scan rate was 2^{o}/min. Further, selected specimens were examined using transmission electron microscopy (TEM; FEI, TECNAI F30) at 300 kV. Electron transparent sections, ~15-nm thick, were obtained using ultramicrotomy. The titanium sheets were too hard to cut by an ultramicrotom with a diamond knife. Thus, the titanium thin films sputtered on aluminum sheets were used as specimens for TEM observations. The titanium films, ~200-nm thick, were prepared using DC magnetron sputtering onto electropolished aluminum specimens. The target used for the preparation of the titanium films was a 99.9 % pure titanium disk. The films were deposited with a current of 0.5 A and voltage of 290 V under an argon pressure of 0.3 Pa; the deposition time was 15 min. The resultant specimens were anodized using the previously described conditions and examined using the TEM. In our previous work, we reported that the crystallinity of the resultant films formed from the sputtered titanium thin films in a hot phosphate/glycerol electrolyte was almost the same as that obtained on a

titanium sheet [11]. The crystal areas and crystal grain sizes were estimated by inverse Fourier-transformed images simulated with the TEM images using Digital Micrograph software (Gatan). The surface and cross-section morphologies of the anodized specimens were observed using scanning electron microscopy (SEM; JEOL, JSM-6500F) operated at 10 kV. In order to estimate the pore size and effective surface area of the anodic films, nitrogen gas adsorption/desorption isotherms (Bel Japan, Belsorp-max instrument) were measured at 77 K. The distribution of pore sizes was analyzed using the BJH method [13], which is useful for mesopores with sizes in the range 2–50 nm.

The photocatalytic activity for decomposition of organic molecules was evaluated on the basis of the decomposition of MB and direct red 80 (DR) in an aqueous solution (pH 5.85, both the molecular formulae are shown in Fig. 1). As displayed in Fig. 1, the molecular size of DR (MW 1373.05, 3.8 nm × 1.2 nm) is much larger than that of MB (MW 319.85, 1.4 nm× 0.6 nm). The molecular sizes were calculated using ChemBio3D software (PerkinElmer Informatics), assuming an all-trans configuration. An aqueous solution containing 10×10^{-5} mol dm^{-3} of each of MB and DR was prepared and the anodized specimens were immersed in 50 ml of it. The solution was stirred for 30 min without UV irradiation to reach the adsorption equilibrium. Then, the TiO_2 nanochannel films were irradiated with the UV light and 2 ml of the mixture was collected every 30 min. The UV irradiation was obtained using the 365-nm band from a 500-W high-pressure xenon lamp (WACOM, HX-504), employing the 33U band-pass filter (ASAHI SPECTRA, UTVAF 50S-33U). The intensity of the UV light was 60 mW cm^{-2}, measured using a thermopile (NEO ARK, PM-335A). The photocatalytic activity was examined by monitoring the reduction of the absorbance

at 682 nm for MB and 508 nm for DR. The spectrophotometric measurements were carried out using a UV/Vis spectrometer (JASCO Corp., JASCO V-550).

3. Results and discussion

Fig. 2 shows the current transients of titanium specimens during anodizing in the hot phosphate/glycerol electrolyte containing 0.03 % water at 20 V for 1 h. In all the electrolytes, the formation voltage of 20 V was rapidly attained during the initial period of anodizing. The subsequent gradual decrease in current in the anodic films with time was typical for anodizing in the hot phosphate/glycerol electrolyte [10,11,14-17], although the porous anodic alumina films formed in aqueous acidic electrolytes showed a steady current density [18]. The most important feature was that the specimens anodized in highly basic electrolytes showed higher anodic current densities. Thus, the growth of the film was faster in the highly basic electrolytes, as discussed later. In the P5 electrolyte, which had the lowest basicity in this study, an anodic film with no measurable thickness was formed, as verified by the cross-sectional observations in the SEM, implying that not the porous layer but the thin barrier layer was formed on the titanium surface. Therefore, we have only discussed below the films anodized in the P1–P4 electrolytes.

Fig. 3 shows the XRD patterns of the films generated after anodizing in the P1, P2, P3, and P4 electrolytes. The sharp peaks of crystalline anatase appeared in all the XRD patterns of the as-anodized specimens. The most intense peak was the 004 peak of anatase in all specimens, whereas the 101 peak for

randomly oriented anatase was missing, as reported previously for the specimen formed in the P3 electrolyte [9-11]. The grain size of the crystal, estimated using the Scherrer's equation for the 004 peak, was approximately 10 nm, regardless of the electrolyte used. This suggested that the orientation of the crystal grains and the grain size were not affected by the basicity of the electrolyte used for anodizing.

Further detailed crystal characterization was carried out using the high-resolution TEM. Fig. 4 shows the transmission electron micrographs of the pore walls of the ultramicrotomed sections anodized in (a), (a)' P1 and (b), (b)' P3 electrolytes. In our previous report, the crystallinity of the TiO_2 film formed by anodizing the sputtered titanium film in the P3 electrolyte was almost the same as that by anodizing a titanium sheet (the morphology of the former one was not exactly the same as the latter one due to the difference of the structure and densification between the sputtered titanium films and the titanium sheets) [11]. The both Fourier-transformed images, shown in Fig. 4 (a) and (b) insets, reveal that the anatase crystal grains were formed and the {001} face of anatase is coincidence with the growth direction of the anodic film as reported previously for the specimen formed in the P3 electrolyte [10]. This result was consistent with those obtained from the XRD. It was evident from the micrographs that the nanocrystals (the areas marked red and green in Fig. 4 (a)' and (b)') were surrounded by an amorphous matrix in both films. We could see that the grain size of the crystal was approximately 10 nm, in agreement with the XRD results. Using the ratios of the crystalline to amorphous regions obtained from the several TEM images of both films, the crystalline areas of the films anodized in the P1 and P3 electrolytes were found to constitute

70.8 % and 71.9 % of the films respectively. These results suggested that the crystallinity of the resultant film was little affected by the basicity of the hot phosphate electrolyte during anodizing.

Fig. 5 shows scanning electron micrographs of the surfaces and cross-sections of the TiO_2 films anodized in P1–P4 electrolytes for 1 h. The images in Fig. 5a-d reveal that porous morphologies were formed on all specimens. The surface appearance became rougher with a decrease in the basicity of the electrolyte. The inset images of Fig. 5e-h show that the thicknesses of the P1, P2, P3, and P4 films anodized for 1 h are 12.5, 9.6, 5.6, and 3.9 μm respectively. Thus, the rate of the film growth increases with the basicity of electrolyte. Table 2 shows the electric charge density (*C*), film thickness (*l*), and thickness/electric charge density (*l*/*C*) of each TiO_2 film. As shown in Table 2, the electric charge density and film thickness increased with the increasing basicity of the electrolyte. However, the *l*/*C* values of P1–P4 were almost the same, implying that the difference in the basicity did not influence the growth efficiency of the TiO_2 nanochannel films. This result was consistent with those obtained from the XRD and TEM analyses because the oxygen-evolution reaction occurred on crystal grains during anodizing [19,20]. Therefore, the largest electric charge density of P1 suggested that a high basicity of the electrolyte accelerated the rate of formation of the film during anodizing. In order to evaluate anodizing in an electrolyte containing NH_4F, Feng et al. studied the influence of electrolyte pH on the rate of formation of the TiO_2 nanotubular films [21]. They reported that the formation rate of the nanotube is rapid in the basic condition compared with acidic conditions. However, in their case, the current density during anodizing did not change with the basicity of the electrolyte. This is because the rate of chemical dissolution, which

is not redox reaction, at the mouth in basic condition was later than that in acidic condition, leading to a higher rate of formation of the anodic nanotubes in basic condition.

On the other hand, the behavior is different in the present case. The current density during anodizing increased with increasing basicity, implying that the high basicity accelerated the formation of the film at the metal/film interface. It is known that during the formation of porous anodic oxides, the formation of the film proceeded at the metal/film interface by the inward migration of O^{2-} ions in the barrier layer under a high electric field; the barrier layer is sandwiched between the porous layer and the metal substrate. For the formation of the porous layer, it has been suggested that the film material does not form at the pore base. Rather, field-assisted dissolution, instead of film formation, occurs at the pore base, resulting in a steady-state thickness of the barrier layer. Another model has been proposed for the flow of film material from the pore base to the pore wall during the growth of the porous anodic amorphous alumina films [22]. However, this appears to be less likely with the TiO_2 nanochannel films because the stress-induced flow may occur in the growing amorphous oxide and the crystalline anatase phase present in the anodic film may hinder the flow of the film material.

During anodizing of niobium in similar hot phosphate/glycerol electrolyte, it was suggested that the growth of the anodic film was controlled by the diffusional transport of matter, probably in developing cylindrical pores [15]. Assuming that the growth of the anodic films on titanium in the present study is also diffusion-controlled, the concentration of diffusing species, probably water or OH^- species, would be

increased in the electrolytes with higher basicity. The detailed study is now in progress and will be reported separately.

Interestingly, the porous morphology was strongly affected by the basicity of the phosphate electrolytes. From Fig. 5e-h, it is evident that films with more regular cylindrical nanochannels developed on increasing the basicity of the electrolytes. Previously, Ono et al. have studied the formation of self-ordered anodic porous alumina films in organic acid electrolytes such as malonic and tartaric acids [23]. They reported that a high current density during anodizing induced a highly ordered cell arrangement of porous alumina films. When the current density is high, a rapid oxide growth induces a compressive force on the barrier layer between each cell boundary. Therefore, the bottommost cells at the barrier layer are pressed against each other under a high current density, leading to a self-ordering behaviour that proceeds simultaneously with the growth of the porous anodic alumina films. In the present work, anodizing in highly basic electrolytes led to a higher current density in the films, suggesting that such a high current density had induced the development of more regular nanochannels.

Because the pore size was not clearly identified using the SEM, the pore size distribution was examined using nitrogen gas adsorption/desorption isotherms. The thickness of each film was 5 μm. Fig. 6 shows the distribution of pore sizes of the films formed in the P1, P3, and P4 electrolytes obtained from nitrogen adsorption isotherms. In this figure, V_p and d_p denote the pore volume and pore diameter respectively. The peak pore diameters of P1, P3, and P4 show basicity-dependence, i.e., lower basicity induced a larger distribution of pore diameters. This result was consistent with the observation that the

ordered porous film was obtained in highly basic conditions (Fig. 5e-h). Ono et al. had reported that when self-ordering of the cell arrangement proceeded for anodic oxide porous films, the cells became smaller, although the applied voltage remained constant [23,24]. Table 3 shows the BET roughness factors of the P1, P3, and P4 specimens calculated using Fig. 6. It is evident that the BET roughness factors of P1 and P3 are smaller than that of P4 because of the smaller distribution in the pore sizes of P1 and P3 compared to that of P4.

Because the anatase nanochannel films anodized in the most basic electrolyte had a small diameter as ~10 nm and sharp pore distribution, the films were used in the size-selective photocatalytic decomposition of organic molecules. Fig. 7 shows the UV-vis spectra of a mixture of MB and DR under UV irradiation for 120 min on (a) the highly ordered P1 film and (b) the NT film. In both the films, the two main peaks at 682 and 508 nm were attributed to the MB and DR molecules respectively. Moreover, a decrease in the intensity of the MB peak was more rapid than that of the DR peak when the P1 film was used as a photocatalyst. Conversely, the intensity of both the peaks of MB and DR decreased at a similar rate when the NT film was used. The insets in Fig. 7 show a comparison of the photocatalytic decomposition rates of MB (λ_{max} = 682 nm) and DR (λ_{max} = 508 nm) with the P1 and NT films. Assuming first-order decomposition kinetics [25,26], $\ln(C/C_0)$ is plotted as a function of photo-irradiation time, t. In the case of the NT film, the decomposition of MB and DR decreased with the UV-irradiation time, suggesting that both molecules could be decomposed on TiO_2 films. This result was consistent with the previously published reports, i.e., in general, TiO_2 could decompose both organic molecules (MB and DR) [25-27]. On

other hand, in the case of P1 nanochannel films, the rate of decomposition of DR was relatively slow while that of MB was comparatively faster on the NT film because of the higher surface area. In the previous report, Ray et al. reported size-selective separation of proteins with different size such as Cytochrome C (12 kDa), Bovine Serum Albumin (69 kDa) and β galactosidase (116 kDa) using anodic TiO_2 nanochannel membrane [28]. On the other hand, in the present study, the anodic TiO_2 nanochannels could select much smaller molecules such as MB and DR than the proteins by precise control of the pore structures.

In most cases, photo-generated holes on TiO_2 reacted with either the surface OH groups or H_2O molecules and generate active hydroxyl radicals, which are usually nonselective oxidants of organic molecules. However, in the case of mesoporous TiO_2 with pore sizes in the range 3–7 nm, Shiraishi et al. reported that the diffusion distance of the hydroxyl radicals formed inside the pores was 1.3–2.4 nm [29]. Therefore, hydroxyl radicals formed inside the pore were deactivated rapidly and, thus, scarcely diffused out of the pores, suggesting that almost all organic molecules were decomposed on the inside wall of the TiO_2 nanochannel films. Of course, few molecules reacted at the surface of the P1 film, but this may be ignored because of the high BET surface roughness of the P1 film. There are two possibilities that induce photocatalytic selectivity: (i) differences in the adsorption properties between the P1 and NT films and (ii) differences in the hindrance of the passage of reactive molecules owing to the difference in pore diameters. Bai et al. reported that the adsorption ratio of MB on TiO_2 increased with an increase of the number of exposed {001} facets [4,5]. The Ti-O-Ti bond angles on the exposed {001} facets were very large and the 2p states on the surface oxygen atoms were destabilized, leading to a facile fabrication of $Ti\text{-}O^-$ species.

Therefore, an ionization atom S^+ in MB was preferentially adsorbed on the reactive Ti-O^- [5]. On the other hand, in our case, the anatase phase with the {001} preferred orientation to the direction of film growth was developed by anodizing in the P1 electrolyte, suggesting that the inside walls of regular nanochannels of the P1 film had less exposed {001} facets than those of the NT film. This implied that the MB molecules containing ionization atoms S^+ were sparsely adsorbed on the P1 film compared with the DR molecules containing ionization groups SO^{3-} on the NT film, indicating that the decomposition rate of MB must have been slower than that of DR. However, this hypothesis was inconsistent with the result shown in Fig. 7. On the other hand, the molecular size of DR (3.8 nm × 1.2 nm) was larger than that of MB (1.4 nm × 0.6 nm) (see Fig. 1). The pore size of the P1 film (~10 nm) was only 2–3 times as large as the molecular size of DR, thereby leading to a decrease in the diffusion rate of DR into the pores of the P1 film compared with that into the pores of the NT film (~100 nm). Therefore, the DR molecules hardly diffused into the nanochannel P1 film while the MB molecules readily diffused into it. On the other hand, in the case of the NT films, the pore diameter was much larger than the molecular sizes of MB and DR. In fact, the P1 films hardly showed the presence of DR molecules in their pores after sintering in 10×10^{-5} mol dm^{-3} DR aqueous solution for 30 min in the dark, whereas the NT films showed the presence of many DR molecules in their pores (Supplementary data, Fig. S1(b),(e)). In addition, it is well known that the surface charge of TiO_2 was strongly dependent on pH of the solution [30,31]. However, the amounts of DR molecules in P1 and NT pores didn't change in wide range of pH, suggesting that the amounts of DR molecules was not strongly affected by the surface charge of inside pores but by the pore sizes of the P1 and NT films

(Supplementary data, Fig. S1). Therefore, the P1 film showed “photodecomposition selectivity” for these organic molecules because of the suppressed diffusion of DR molecules into the pores.

4. Conclusions

Crystalline anatase TiO_2 nanochannel films are formed by anodizing titanium in various basic electrolytes containing phosphates. The crystallinity of the anodic films was not affected by the basicity of the electrolytes. On the other hand, the growth rate of the films increased with an increase in the basicity of the electrolyte. In addition, as the growth rate increased, leading to highly ordered nanochannel structures. In addition, the highly ordered TiO_2 nanochannel film showed selectivity in the photodecomposition of organic molecules. In general, TiO_2 shows high photo-oxidized activity for water and organic molecules, thereby leading to low photo-oxidized selectivity. The present work has discovered a new photochemical property of anodized TiO_2 films by accurate control of the porous structures. We believe that highly ordered nanochannel structures can have various practical applications in the fields of biosensors and artificial photosynthesis.

Acknowledgements

The present work was supported by the JSPS Grant-in-Aid for Young Scientists (B) (Grant Number 25810132) and JSPS Institutional Program for Young Researcher Overseas Visits. The authors also acknowledge the support provided by the EPSRC LATEST2 Programme Grant.

References

[1] T. Tachikawa, M. Fujitsuka, T. Majima, Mechanistic Insight into the TiO_2 Photocatalytic Reactions: Design of New Photocatalysts, J. Phys. Chem. C 111 (2007) 5259-5275.

[2] J.-M. Herrmann, Heterogeneous Photocatalysis: State of the Art and Present Applications In Honor of Pr. R.L. Burwell Jr. (1912–2003), Former Head of Ipatieff Laboratories, Northwestern University, Evanston (Ill), Top. Catal. 34 (2005) 49-65.

[3] Y. Shiraishi, D. Tsukamoto, T. Hirai, Selective Photocatalytic Transformations on Microporous Titanosilicate ETS-10 Driven by Size and Polarity of Molecules, Langmuir 24 (2008) 12658-12663.

[4] Y. Bai, P. Luo, P. Wang, J. Liu, Synthesis of Uniform Anatase TiO_2 Microspheres with Exposed {001} Facets: Without HF Utilization and Its Photocatalytic Selectivity, Catal. Commun. 37 (2013) 45-49.

[5] J. Zhang, W. Chen, J. Xi, Z. Ji, {001} Facets of Anatase TiO_2 Show High Photocatalytic Selectivity, Mater. Lett. 79 (2012) 259-262.

[6] S. Liu, J. Yu, M. Jaroniec, Tunable Photocatalytic Selectivity of Hollow TiO_2 Microspheres Composed of Anatase Polyhedra with Exposed {001} Facets, J. Am. Chem. Soc. 132 (2010) 11914-11916.

[7] M. Yasui, K. Katagiri, S. Yamanaka, K. Inumaru, Molecular Selective Photocatalytic Decomposition of Alkylanilines by Crystalline TiO_2 Particles and their NanocompoSites with Mesoporous Silica, RSC Adv. 2 (2012) 11132-11137.

[8] K. Inumaru, M. Yasui. T. Kasahara, K. Yamaguchi, A. Yasuda, S. Yamanaka, Nanocomposites of Crystalline TiO_2 Particles and Mesoporous Silica: Molecular Selective Photocatalysis Tuned by Controlling Pore Size and Structure, J. Mater. Chem. 21 (2011) 12117-12125.

[9] H. Habazaki, M. Teraoka, Y. Aoki, P. Skeldon, G.E. Thompson, Formation of Porous Anodic Titanium Oxide Films in Hot Phosphate/glycerol Electrolyte, Electrochim. Acta 55 (2010) 3939-3943.

[10] Y. Taguchi, E. Tsuji, Y. Aoki, H. Habazaki, Photo-induced Properties of Non-annealed Anatase TiO_2 Mesoporous Film Prepared by Anodizing in the Hot Phosphate/glycerol Electrolyte, Appl. Surf. Sci. 258 (2012) 9810-9815.

[11] E. Tsuji, N. Hirata, Y. Aoki, H.Habazaki, Preparation of Non-annealed Anatase TiO_2 Film on ITO Substrate by Anodizing in Hot Phosphate/glycerol Electrolyte for Dye-sensitized Solar Cells, Mater. Lett. 91 (2012) 39-41.

[12] K. Fushimi, H. Habazaki, Anodic Dissolution of Titanium in NaCl-containing Ethylene Glycol, Electrochim. Acta 53 (2008) 3371-3376.

[13] E.P. Barrett, L.G. Joyner, P.P. Halenda, The Determination of Pore Volume and Area Distributions in Porous Substances. I. Computations from Nitrogen Isotherms Computations from Nitrogen Isotherms, J. Am. Chem. Soc. 73 (1951) 373380.

[14] H. Habazaki, Y. Oikawa, K. Fushimi, K. Shimizu, S. Nagata, P. Skeldon, G.E. Thompson, Formation of Porous Anodic Films on Ti-Si Alloys in Hot Phosphate-glycerol Electrolyte, Electrochim. Acta 53 (2007) 1775-1781.

[15] Y. Oikawa, K. Fushimi, Y. Aoki, H. Habazaki, Growth of Porous Anodic Films on Niobium in HotPphosphate-glycerol Electrolyte, ECS Transactions 16 (2008) 345-351.

[16] S. Yang, Y. Aoki, H. Habazaki, Effect of Electrolyte Temperature on the Formation of Self-organized Anodic Niobium Oxide Microcones in Hot Phosphate-glycerol Electrolyte, Appl. Surf. Sci. 257 (2011) 8190-8195.

[17] S. Yang, H. Habazaki, T. Fujii, Y. Aoki, P. Skeldon, G.E. Thompson, Control of Morphology and Surface Wettability of Anodic Niobium Oxide Microcones Formed in Hot Phosphate-glycerol Electrolytes, Electrochim. Acta 56 (2011) 7446-7453.

[18] H. Habazaki, Y. Oikawa, K. Fushimi, Y. Aoki, K. Shimizu, P. Skeldon, G.E. Thompson, Importance of Water Content in Formation of Porous Anodic Niobium Oxide Films in Hot Phosphate–glycerol Electrolyte, Electrochim. Acta 54 (2009) 946-951.

[19] H. Habazaki, M. Uozumi, H. Konno, K. Shimizu, P. Skeldon G.E. Thompson, Crystallization of Anodic Titania on Titanium and its Alloys, Corros. Sci. 45 (2003) 2063-2073.

[20] A. Mazzarolo, M. Curioni, A. Vicenzo, P. Skeldon, G.E. Thompson, Anodic Growth of Titanium Oxide: Electrochemical Behaviour and Morphological Evolution, Electrochim. Acta 57 (2012) 288-295.

[21] X. Feng, J.M. Macak, P. Schmuki, Robust Self-organization of Oxide Nanotubes over a Wide pH Range, Chem. Mater. 19 (2007) 1534-1536.

[22] S.J. Garcia-Vergara, P. Skeldon, G.E. Thompson, H. Habazaki, A Tracer Investigation of Chromic Acid Anodizing of Aluminium, Surf. Interface Anal. 39 (2007) 860-864.

[23] S. Ono, M. Saito H. Asoh, Self-ordering of Anodic Porous Alumina Formed in Organic Acid Eletrolytes, Electrochim. Acta 51 (2005) 827-833.

[24] S. Ono, M. Saito, H. Asoh, Self-Ordering of Anodic Porous Alumina Induced by Local Current Concentration: Burning, Solid State Lett.7 (2004) B21-B24.

[25] J.M. Macak, M. Zlamal, J. Krysa, P. Schmuki, Self-organized TiO_2 Nanotube Layers as Highly Efficient Photocatalysts, Small 3 (2007) 300-304.

[26] Y. Xie, Photoelectrochemical Application of Nanotubular Titania Photoanode, Electrochim. Acta 51 (2006) 3399-3406.

[27] S. Tangestaninejad, M. Moghadam, V. Mirkhani, I. M.-Baltork H. Salavati, Sonochemical and Visible Light Induced Photochemical and Sonophotochemical Degradation of Dyes Catalyzed by Recoverable Vanadium-containing Polyphosphomolybdate Immobilized on TiO_2 Nanoparticles, Ultrason. Sonochem. 15 (2008) 815-822.

[28] P. Ray, T. Dey K. Lee, D. Kim, B. Fabry, P. Schmuki, Size-Selective Separation of Macromolecules by Nanochannel Titania Membrane with Self-Cleaning (Declogging) Ability, J. Am. Chem. Soc. 132 (2010) 7893-7895.

[29] Y. Shiraishi, N. Saito T. Hirai, Adsorption-Driven Photocatalytic Activity of Mesoporous Titanium Dioxide, J. Am. Chem. Soc. 127 (2005) 12820-12822.

[30] A. Imanishi, T. Okamura, N. Ohashi, R. Nakamura, Y. Nakato, Mechanism of Water Photooxidation Reaction at Atomically Flat TiO_2 (Rutile) (110) and (100) Surfaces: Dependence on Solution pH, J. Am. Chem. Soc. 129 (2007) 11569-11578.

[31] R. Nakamura, T. Okamura, N. Ohashi, A. Imanishi, Y. Nakato, Molecular Mechanisms of Photoinduced Oxygen Evolution, PL Emission, and Surface Roughening at Atomically Smooth (110) and (100) n-TiO_2 (Rutile) Surfaces in Aqueous Acidic Solutions, J. Am. Chem. Soc. 127 (2005) 12975-12983.

Figure captions

Fig. 1. Chemical structure of dyes, (a) methylene blue (MB) and (b) direct red 80 (DR). Molecular sizes were calculated using ChemBio3D software, assuming an all-trans configuration.

Fig. 2. Current transients of titanium during anodizing at 20 V in (a) 0.6 mol dm^{-3} K_3PO_4 + 0.2 mol dm^{-3} K_2HPO_4 (P1), (b) 0.4 mol dm^{-3} K_3PO_4 + 0.4 mol dm^{-3} K_2HPO_4 (P2), (c) 0.2 mol dm^{-3} K_3PO_4 + 0.6 mol dm^{-3} K_2HPO_4 (P3), (d) 0.4 mol dm^{-3} K_2HPO_4 + 0.4 mol dm^{-3} KH_2PO_4 (P4), and (e) 0.2 mol dm^{-3} K_2HPO_4 + 0.6 mol dm^{-3} KH_2PO_4 (P5) glycerol electrolyte containing 0.03 mass% water at 433 K for 1 h.

Fig. 3. X-ray diffraction patterns of films formed by anodizing in (a) P1, (b) P2, (c) P3, and (d) P4 electrolytes. The thickness of the individual films is 5 μm.

Fig. 4. Transmission electron micrographs of ultramicrotomed sections of films anodized in (a),(a)’ P1

and (b),(b)’ P3 electrolytes. The insets of (a) and (b) are the Fourier-transformed images simulated with the images (a) and (b) using Digital Micrograph software (Gatan). White arrows show the growth direction of the anodic films. Areas marked with (a)’ red and (b)’ green show crystalline nanograins of (a) and (b).

Fig. 5. Scanning electron micrographs of the surfaces and fractured cross-sections of films anodized in (a),(e) P1; (b),(f) P2; (c),(g) P3; and (d),(h) P4 electrolytes for 1 h. Insets of (e) - (h) are low magnification images of cross sections.

Fig. 6. Distribution of pore sizes in films anodized in (a) P1, (b) P3, and (c) P4 electrolytes with 5 μm thick anodic films. Distributions were obtained from nitrogen adsorption isotherms at 77 K.

Fig. 7. Time-dependent UV-Vis spectra of methylene blue (MB) and direct red 80 (DR) mixture during UV irradiation on (a) P1 film, and (b) NT film for 120 min. Insets on the right-hand-sides show scanning electron micrographs of P1 and NT films. The left-hand-side insets show kinetic data for MB (λmax = 682 nm, blue dots) and DR (λmax = 508 nm, pink dots).

List of figures

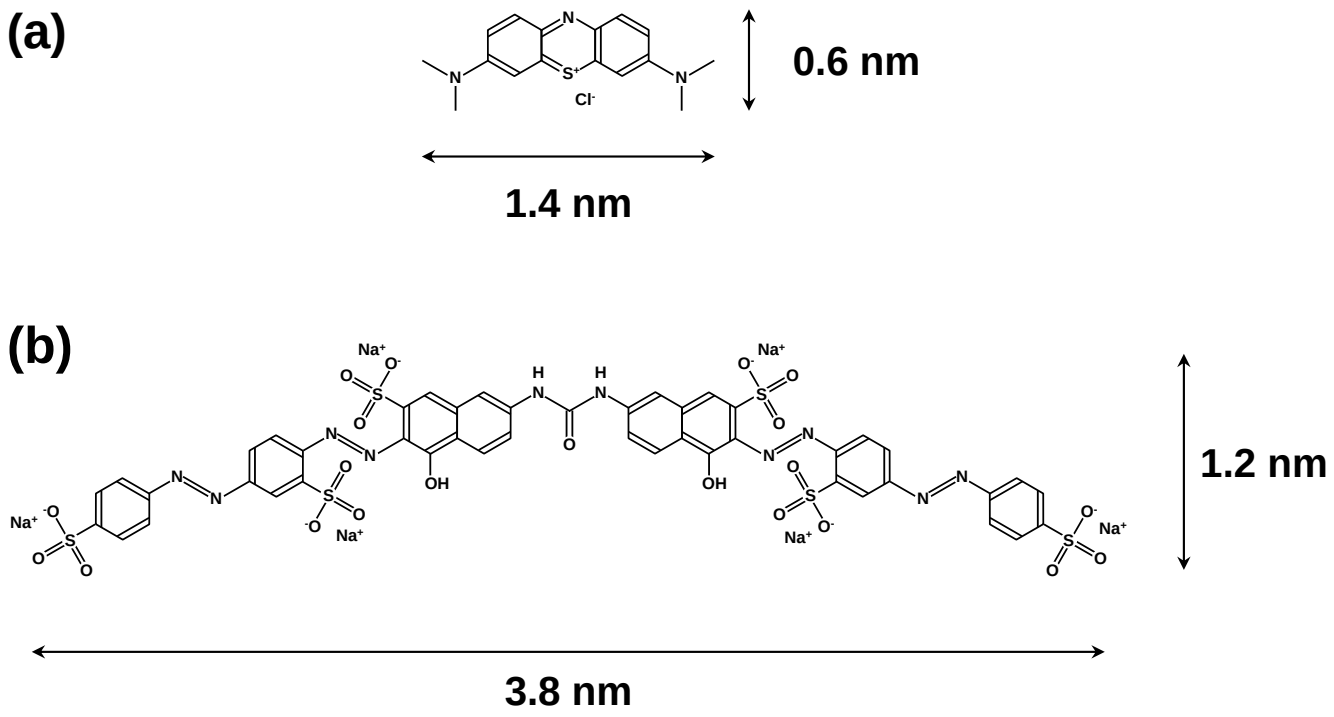

Fig. 1. E. Tsuji, et al.

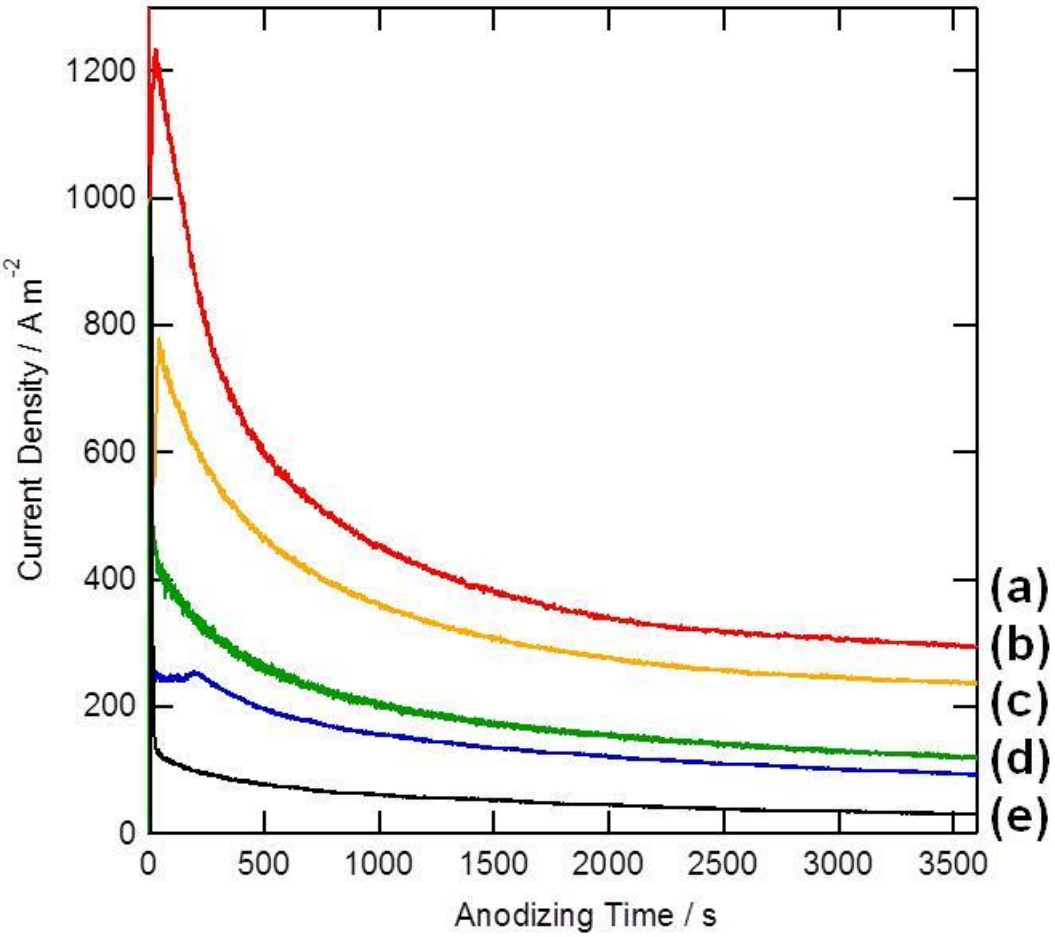

Fig. 2. E. Tsuji, et al.

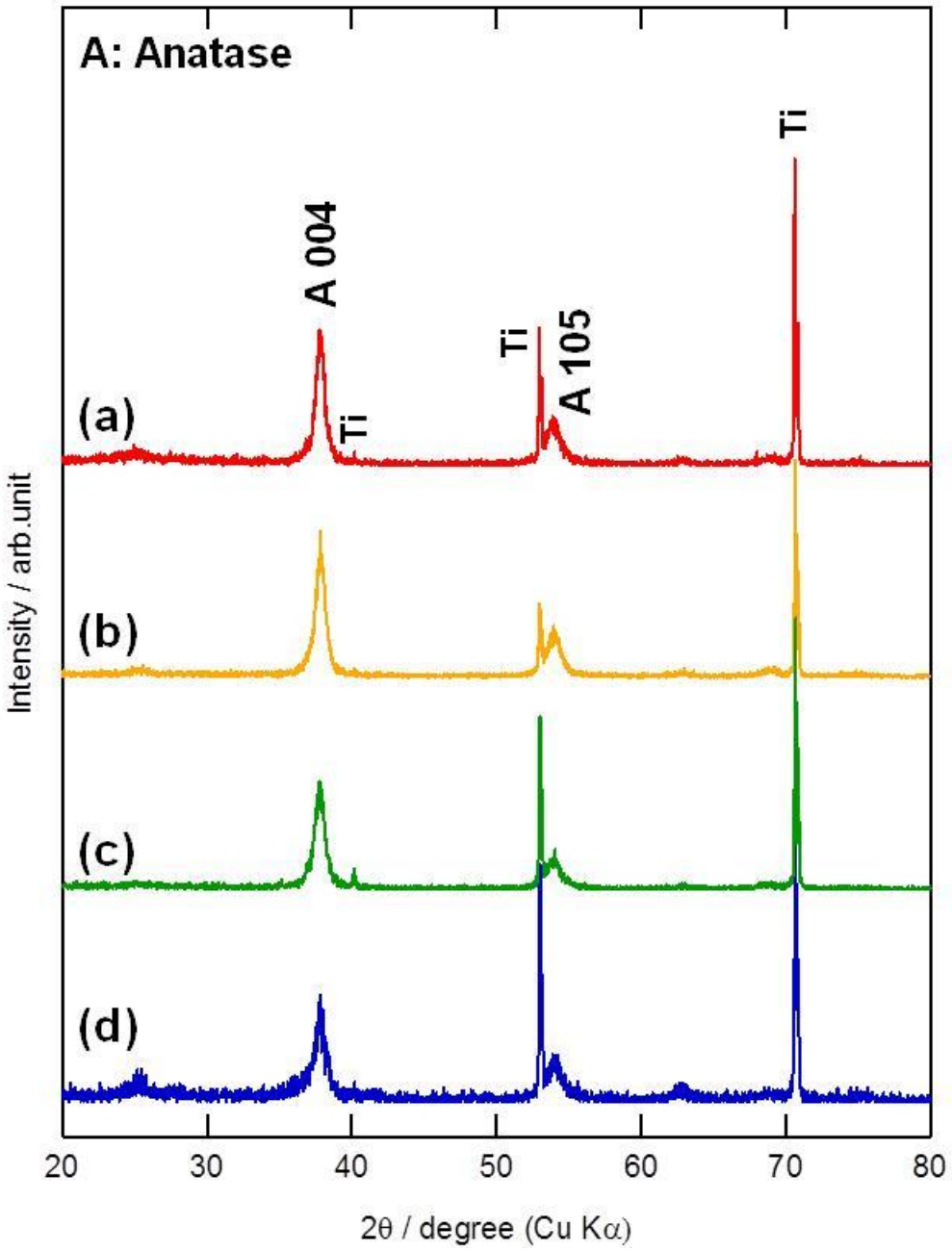

Fig. 3. E. Tsuji, et al.

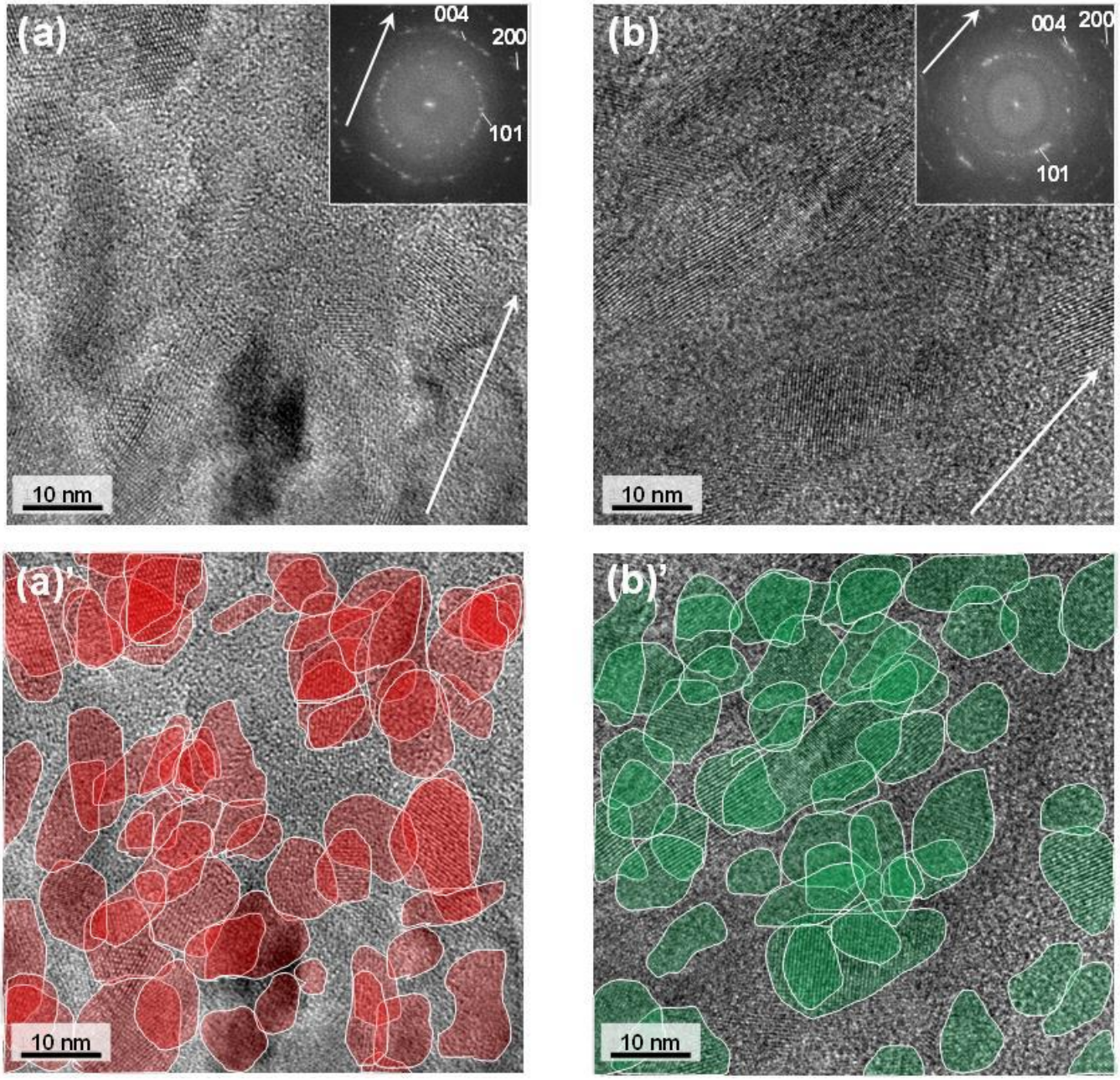

Fig. 4. E. Tsuji, et al.

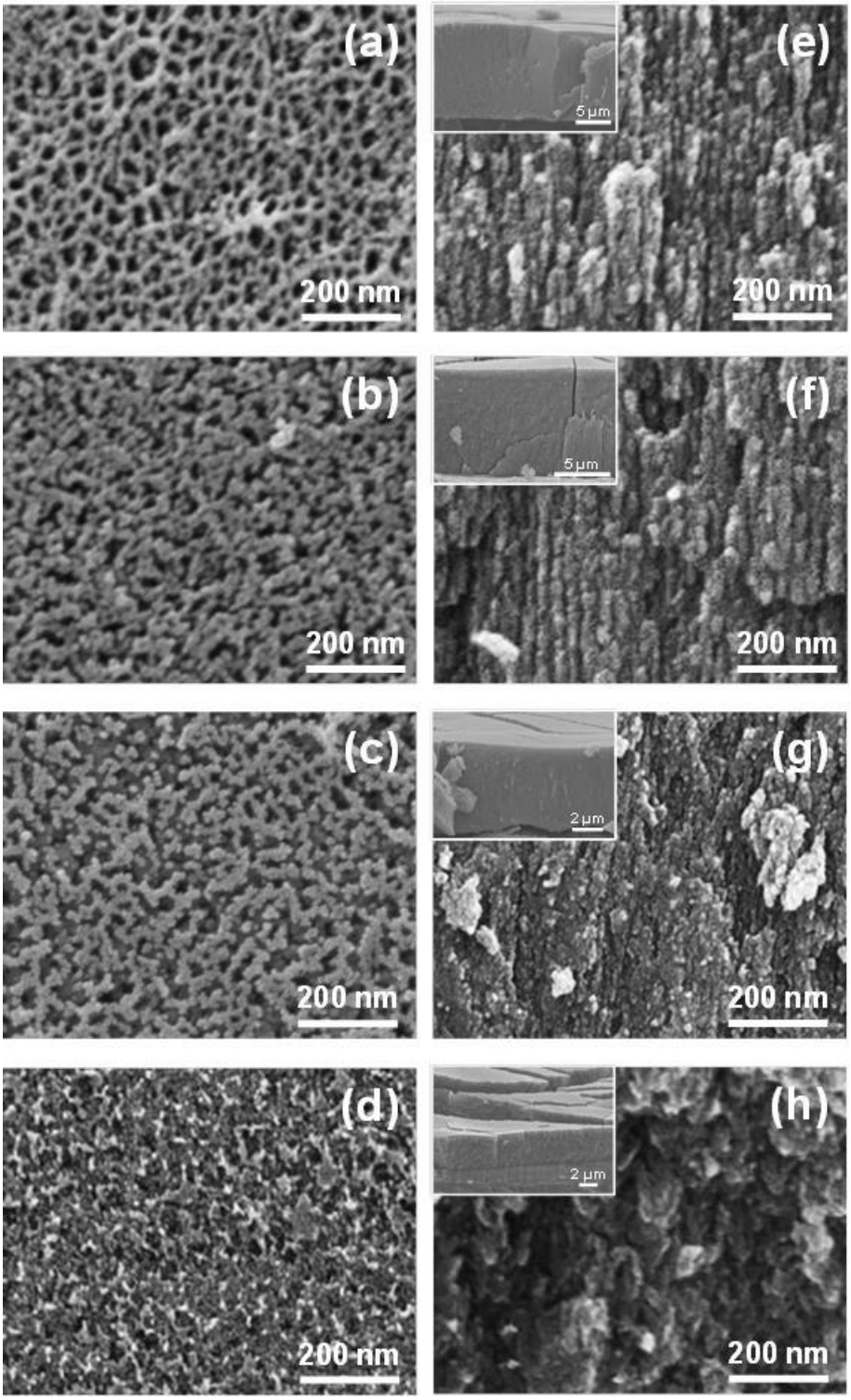

Fig. 5. E. Tsuji, et al.

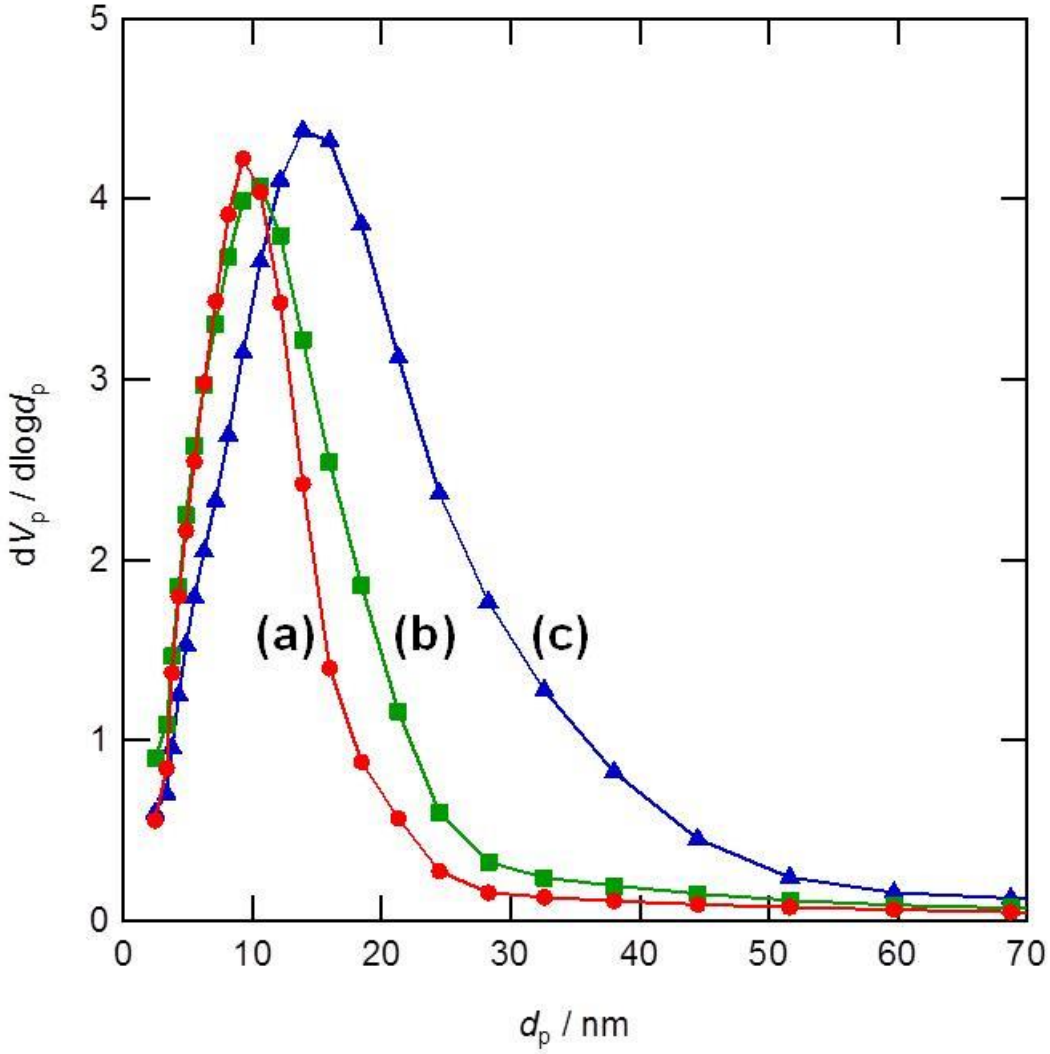

Fig. 6. E. Tsuji, et al.

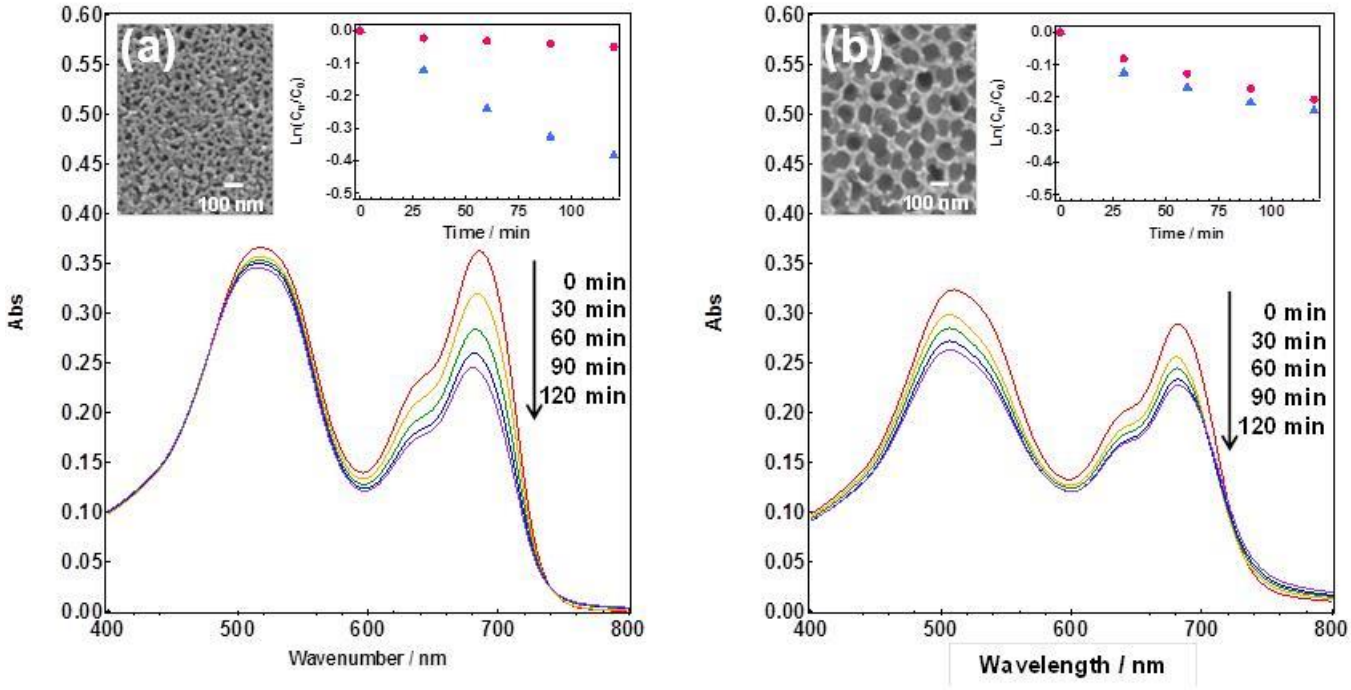

Fig. 7. E. Tsuji, et al.

List of tables

Table 1. Composition of phosphate electrolytes used for anodizing. Total concentration of phosphates was 0.8 mol dm^{-3}.

	P1	P2	P3	P4	P5
K_3PO_4 / mol dm^{-3}	0.6	0.4	0.2	-	-
K_2HPO_4 / mol dm^{-3}	0.2	0.4	0.6	0.4	0.2
KH_2PO_4 / mol dm^{-3}	-	-	-	0.4	0.6

Table 1. E. Tsuji, et. al.

Table 2. Electric charge density (*C*), film thickness (*l*), and thickness/electric charge density (*C*/*l*) of the anodized in P1–P5 electrolytes for 1 h at 20 V.

	P1	P2	P3	P4	P5
Electric charge density(*C*) (kC m^{-2})	1405	1209	672	510	197
Film thickness (*l*) (μm)	12.5	9.6	5.6	3.9	-
l/*C* (10^{-12} m^3 C^{-1})	8.9	7.9	8.4	7.6	-

Table 2. E. Tsuji, et. al.

Table 3. BET roughness factor of films anodized in P1, P3, and P4 electrolytes. The thickness of the individual films is 5 μm.

	P1	P3	P4
Roughness factor	618	650	437

* BET roughness factor of the NT films: 174 [10]

Table 3. E. Tsuji, et. al.

Supplementary data

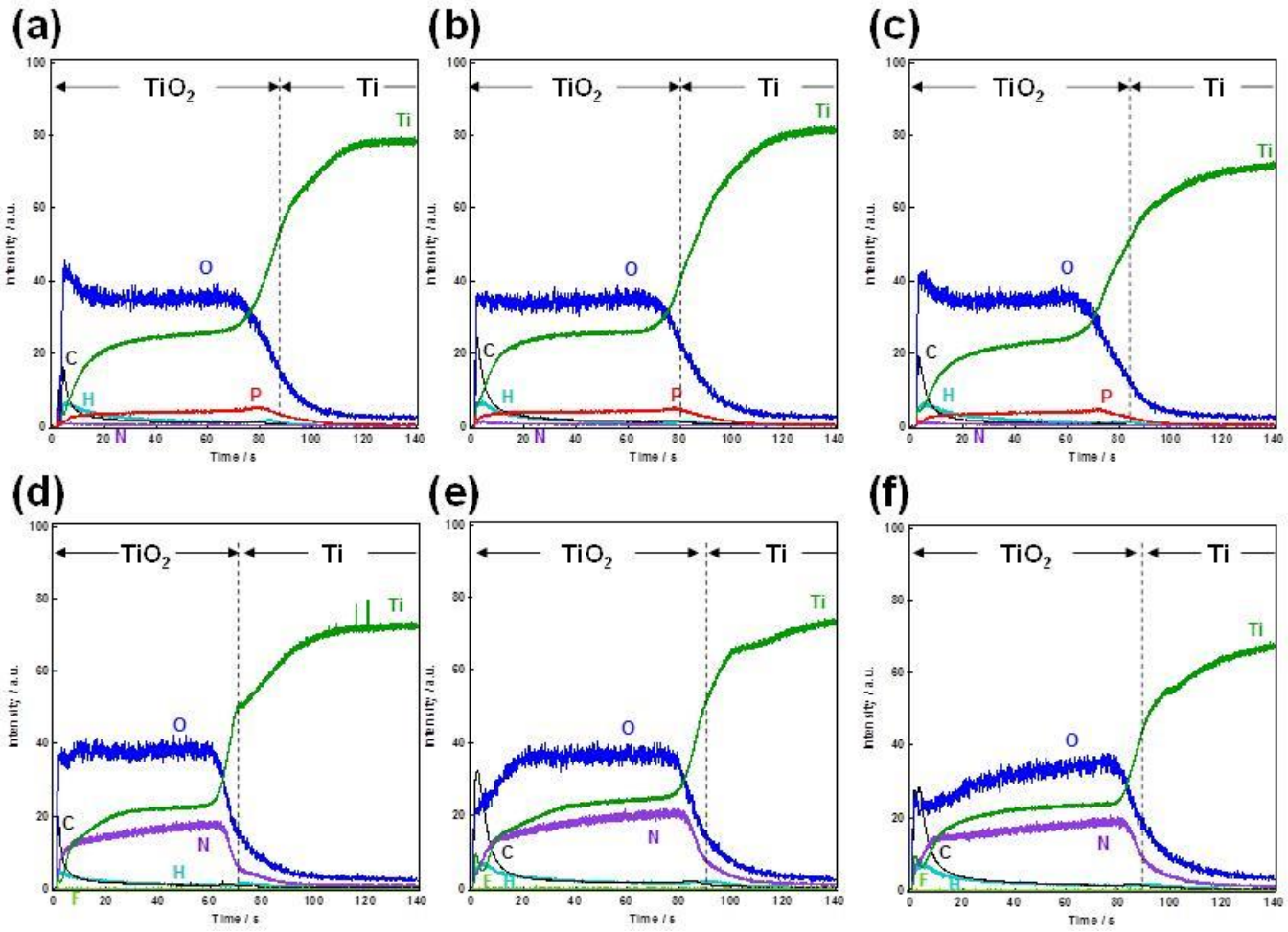

Fig. S1. GDOES depth profiles of (a)-(c) P1 films and (d)-(f) NT films after sintering in mixture of 10 × 10^{-5} mol dm^{-3} DR (a),(d) acidic (pH 1.47), (b),(e) neutral (pH 5.85) and (c),(f) basic (pH 12.73) aqueous solution for 30 min in the dark. pH of DR aqueous solutions were controlled by using 0.1 mol dm^{-3} $HClO_4$ and 0.1 mol dm^{-3} NaOH aqueous solutions for (a),(d) and (c),(f). All P1 films showed almost no intensity of nitrogen in DR, whereas all NT films showed a high intensity of nitrogen. The intensity of nitrogen didn't change with changing pH of the DR aqueous solutions in both films.